

Supporting information

Sensitive NMR Approach for Determining the Binding Mode of Tightly Binding Ligand
Molecules to Protein Targets

Wan-Na Chen, Christoph Nitsche, Kala Bharath Pilla, Bim Graham, Thomas Huber, Christian D.
Klein, Gottfried Otting*

Table S1. PCSs measured of backbone amide protons of DENpro in complex with ligand 1.^a

Residue	Site A		Site B		Site C	
	Tm ³⁺	Tb ³⁺	Tm ³⁺	Tb ³⁺	Tm ³⁺	Tb ³⁺
NS2B						
Ser70*	-0.35	0.46	-0.06	0.08	-0.01	0
Ser71*	-0.26	0.33	-0.05	0.06	-0.02	0.02
Ile73*	-	-	-0.05	0.07	-0.08	0.09
Leu74*	-0.12	0.18	-0.06	0.09	-0.05	0.08
Ser75*	-0.09	0.11	-0.06	0.08	-0.06	0.09
Ile78*	-0.07	-	-0.11	0.17	-0.09	0.20
Ser79*	-0.01	0.02	-0.21	0.25	-0.23	0.34
Asp81*	-	-	-	0.33	-0.34	-0.54
Gly82*	-	-	-0.26	0.33	-0.37	0.58
Ser83*	-	-	-0.34	0.42	-0.31	0.48
Ser85*	-0.03	0.05	-0.16	0.20	-0.14	0.21
Ile86*	-0.05	-	-0.11	0.12	-0.09	0.14
Lys87*	-0.05	0.08	-0.07	0.08	-0.08	0.11
NS3pro						
Gly21	0.58	-	0.16	-0.19	-	-
Ala22	-	-	0.18	-0.22	-	-
Tyr23	-	-	0.32	-0.38	-	-
Lys28	-	-	-	-	0.31	-0.53
Ser34	-	-	-	-	0.21	-

Gly39	0.83	-0.99	0.37	-0.44	0.49	-0.76
Tyr41	0.59	-0.72	0.20	-0.23	0.56	-0.84
Lys42	0.20	-0.25	0.15	-0.17	-	-
Glu43	0.04	-0.06	0.10	-0.12	-	-
Gly44	0.14	-0.19	0.12	-0.16	-	-
Phe46	0.26	-0.30	0.20	-0.23	-	-
Trp50	0.10	-0.12	-	-	-	-
His51	0.12	-0.14	-	-	-0.32	0.05
Val52	0.19	-0.23	-	-	-0.03	-
Thr53	0.24	-0.29	-	-	0.14	-0.26
Gly55	0.19	-0.23	-	-	-	-
Gly62	0.47	-0.58	0.38	-0.44	-	-1.26
Glu66	0.23	-	0.24	-	-	-
Ala70	0.05	-0.05	-0.05	0.05	-	-
Ser78	-	-	0.06	-0.07	-	-
Gly81	0.14	-0.15	0.12	-0.16	-	-
Gly82	0.05	-0.06	0.07	-0.08	-	-
Leu85	-	0.10	0.05	-0.04	-	-
Trp89	-	-	-0.03	0.03	-0.06	0.08
Gly92	-0.28	0.37	-	-	-0.03	0.04
Gln96	-	-	-	-	0.04	-0.07
Leu98	-1.15	-	-	-	0.10	-0.17
Leu100	-	-	-	-	0.17	-0.26

Gly103	-	-	-	-	0.16	-0.26
Gln110	-	-	-0.03	0.05	0.03	-0.06
Thr111	-	1.18	-0.04	0.06	-	-
Gly114	-0.28	-	-0.08	0.08	-	-
Phe116	-0.15	0.21	-0.09	0.10	-0.08	0.11
Lys117	-	-	-0.08	0.09	-0.07	0.11
Thr120	-0.06	0.08	-0.07	0.09	-0.12	0.19
Gly121	-0.07	0.10	-0.06	0.08	-0.11	0.15
Thr122	-	-	-0.05	0.07	-0.10	0.14
Ile123	-	-	-	-	-0.12	0.11
Ser127	-0.36	-	-0.09	0.11	-	-
Val140	-	-	-	-	0.06	-0.10
Gly148	-0.38	0.49	-	-	0.02	-0.06
Ala160	-0.11	0.15	-0.04	0.05	-0.03	0.05
Ala164	-	-	-0.22	0.28	-0.08	0.12
Ile165	-	-	-0.12	0.14	-	-
Ala166	-	-	-0.08	-	-0.08	0.13

^a PCSs were generated by C2-Tm³⁺ and C2-Tb³⁺ tags at sites A-C. Corresponding samples with C2-Y³⁺ tags were used as the diamagnetic reference. PCSs are reported in ppm as the ¹H chemical shift measured in the presence of paramagnetic tag minus the ¹H chemical shift measured of the diamagnetic reference.

Table S2. PCSs observed in NOESY spectra of the complex between ligand **1** and DENpro with C2-Ln³⁺ tags^a

Tag site and metal	Ligand 1			Protein		
	<i>tert</i> -butyl group	H-1/1'	H-2/2'	CH ₃ -1	CH ₃ -2	H-3
	(ppm)	(ppm)	(ppm)	(ppm)	(ppm)	(ppm)
A-Tm ³⁺	-0.01	0.00	0.00	-0.05	-0.06	-0.05
A-Tb ³⁺	0.02	0.01	0.01	0.07	0.09	0.08
B-Tm ³⁺	-0.09	-0.27	-0.56	-0.14	n.d.	n.d.
B-Tb ³⁺	0.10	0.33	0.67	0.15	n.d.	n.d.
C-Tm ³⁺	-0.10	-0.10	-0.10	-0.06	-0.05	-0.06
C-Tb ³⁺	0.16	0.16	0.16	0.09	0.07	0.10
Chemical shift ^a	1.30	7.54	7.66	0.67	0.78	1.73

^a Measured for the complex of ligand **1** with wild-type DENpro without tag. See Figures 1A and 2B for the numbering of the proton resonances. n.d., not detected.

Table S3. $\Delta\chi$ tensor parameters fitted to the homology model built of DENpro and refined by Rosetta^a

Tagging site and metal	$\Delta\chi_{ax}$	$\Delta\chi_{rh}$	x	y	z	α	β	γ
A-Tm ³⁺	17.1	6.7	16.415	-18.172	36.099	140.1	139.5	38.5
A-Tb ³⁺	-21.1	-8.3	16.415	-18.172	36.099	141.4	139.8	42.7
B-Tm ³⁺	8.7	2.0	8.634	-21.149	7.976	102.9	54.8	43.0
B-Tb ³⁺	-10.5	-2.7	8.634	-21.149	7.976	102.5	56.8	41.8
C-Tm ³⁺	17.7	3.5	13.935	4.362	4.462	49.3	147.9	82.2
C-Tb ³⁺	-27.4	-6.9	13.935	4.362	4.462	49.3	147.9	82.2

^a The tensor parameters are reported with respect to the final Rosetta-refined model, which is available from <http://rsc.anu.edu.au/~go/coordinates/>. The axial and rhombic components of the $\Delta\chi$ tensors are given in 10^{-32} m^3 and the Euler angles in degrees, using the zyz convention and unique tensor representation.¹ $\Delta\chi$ tensor fits were performed by restricting Tb³⁺ and Tm³⁺ to the same site.

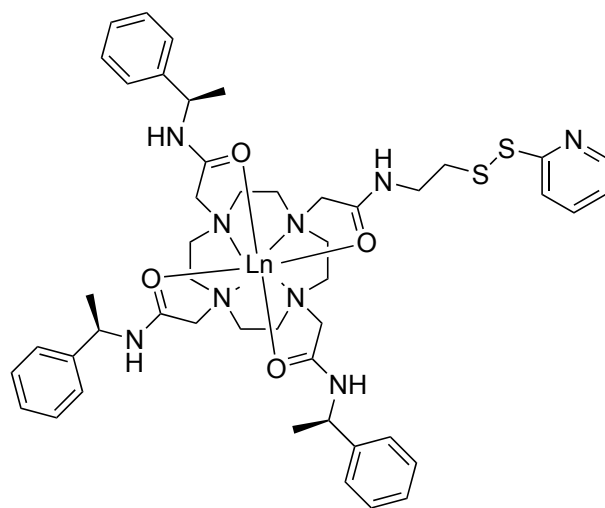


Figure S1. Chemical structure of the C2-Ln³⁺ tag.²

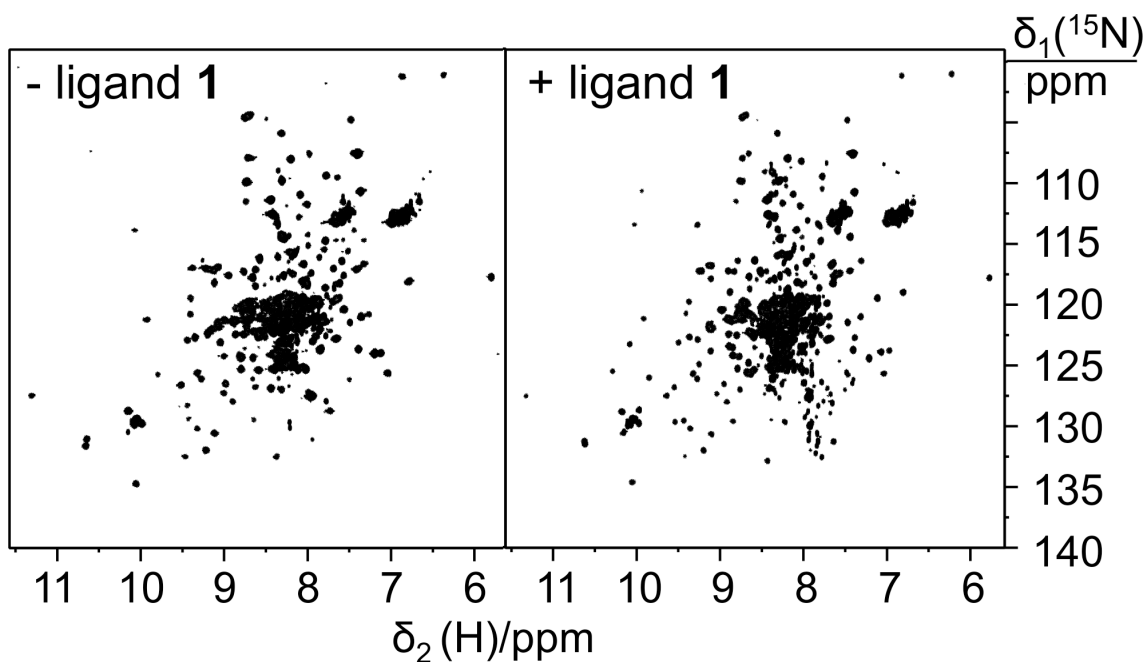


Figure S2. ^{15}N -HSQC spectra of DENpro without (left spectrum) and with ligand **1** (right spectrum). The spectra were recorded of 150 μM solutions of uniformly ^{15}N -labeled DENpro tagged at site B with a diamagnetic C2-Y^{3+} tag. The comparison shows that many of the well-resolved peaks can be tracked despite some changes in chemical shifts.

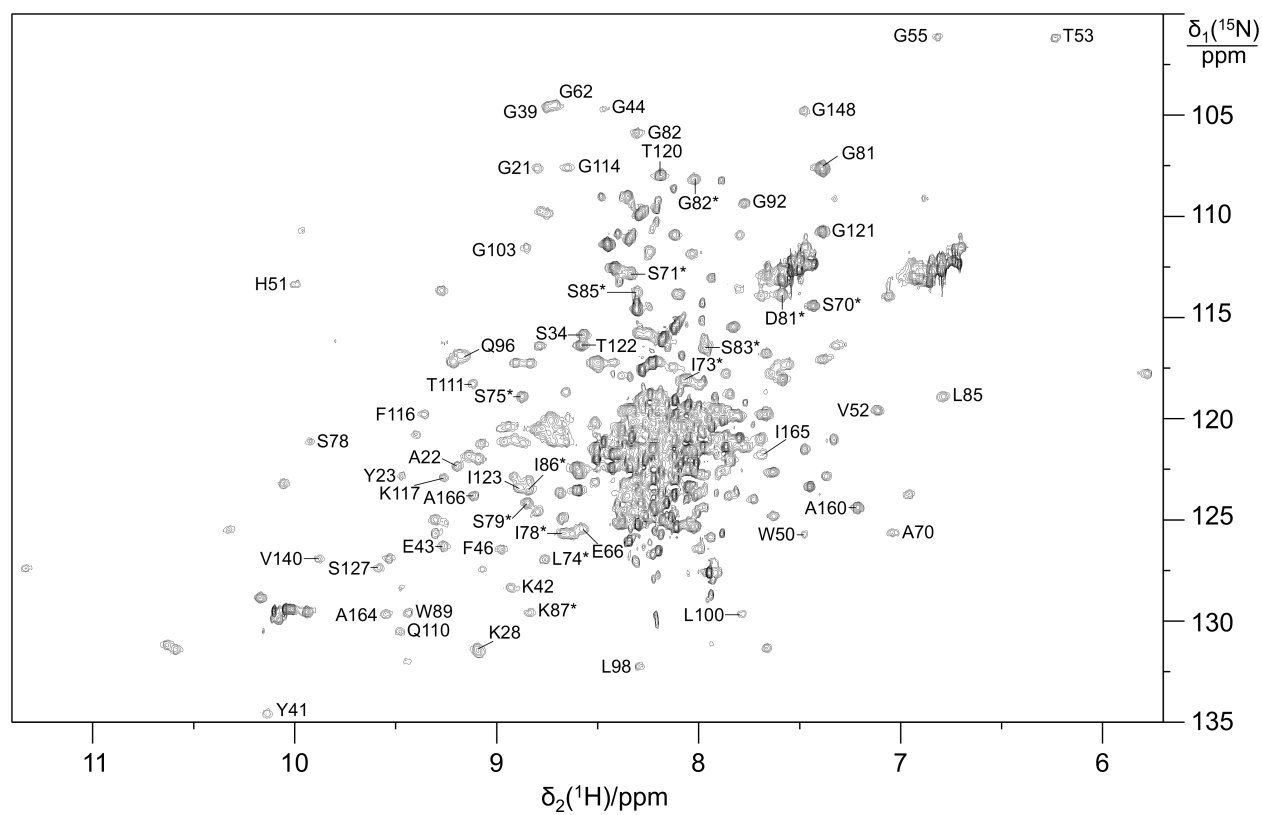


Figure S3. ^{15}N -HSQC spectrum recorded of a 150 μM solution of uniformly ^{15}N -labeled DENpro tagged at site A with a diamagnetic C2-Y^{3+} tag and in complex with ligand **1**. Solution conditions: 20 mM MES, pH 6.5, 50 mM NaCl, 25 $^{\circ}\text{C}$. The spectrum was recorded using a 3 mm NMR tube on a Bruker 800 MHz NMR spectrometer equipped with a TCI cryoprobe. The cross-peaks used as diamagnetic reference for PCS measurements (Table S1) are marked with their sequence-specific residue assignments.

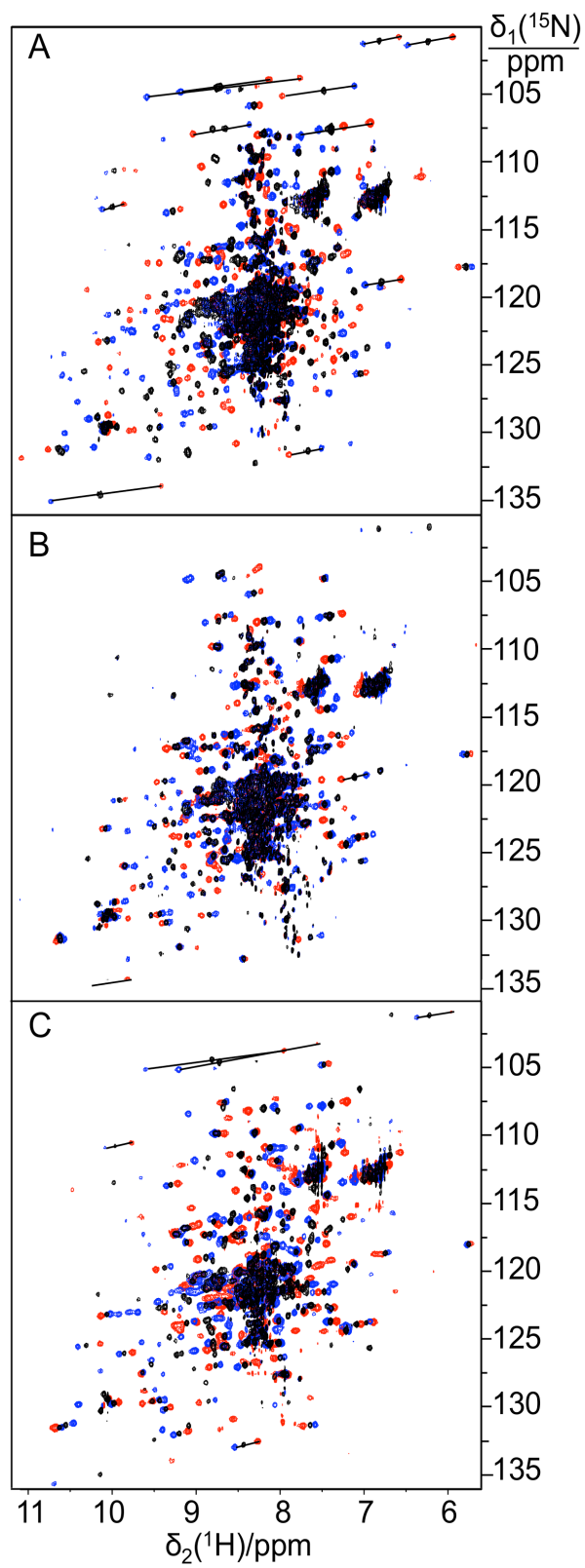


Figure S4. PCS measurements of backbone amide protons. The figure shows superimpositions of ^{15}N -HSQC spectra recorded of uniformly ^{15}N -labeled DENpro in complex with ligand **1** with

C2-Ln³⁺ tags at different sites of DENpro. Panels A-C show the spectra with tags at sites A, B, and C, respectively. Spectra of DENpro with diamagnetic tag (C2-Y³⁺) are shown in black, and the corresponding spectra with paramagnetic tags are plotted in red (C2-Tm³⁺) and blue (C2-Tb³⁺). Selected cross-peaks are linked by lines indicating the pseudocontact shifts. The spectra were recorded of 150 μM solutions of DENpro-ligand **1** complexes in NMR buffer (pH 6.5) at 25 °C, using a Bruker 800 MHz NMR spectrometer. Based on the cross-peaks observed in these ¹⁵N-HSQC spectra, the tag ligation yields at sites A-C were about 80%, 70%, and 90%, respectively.

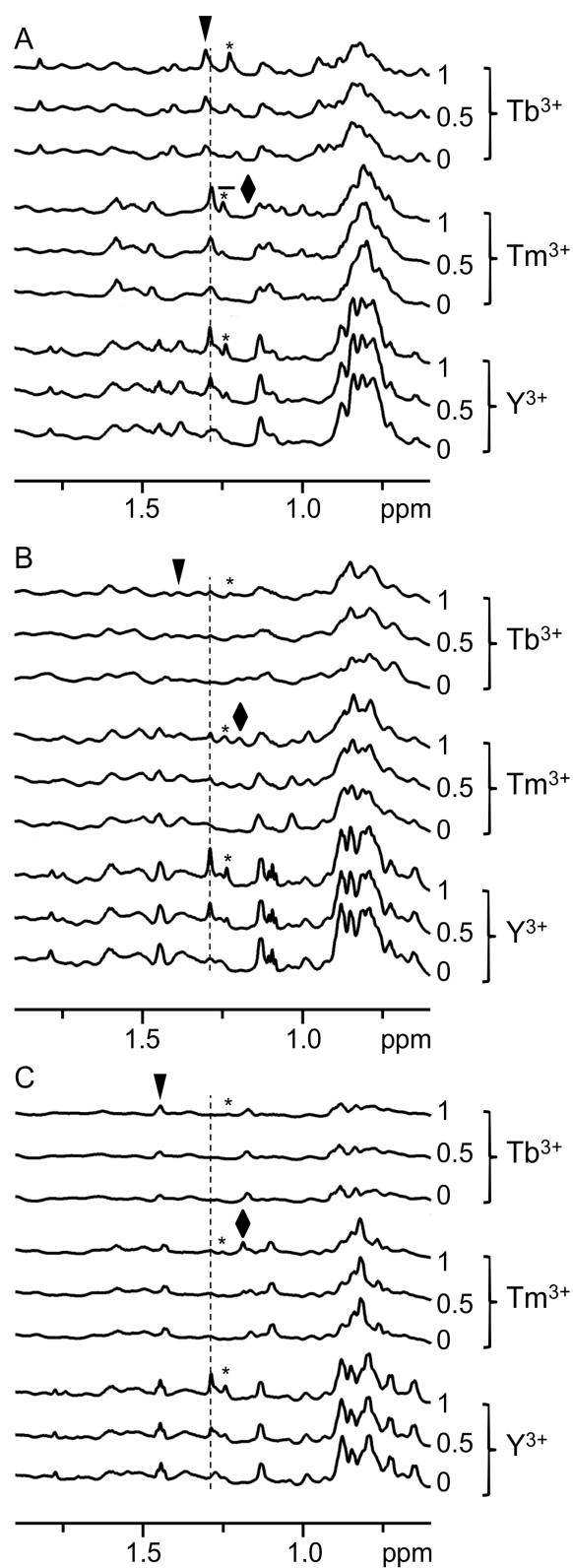


Figure S5. PCSs of the *tert*-butyl signal observed in 1D ^1H NMR spectra measured of ligand **1** in complex with DENpro with different C2- Ln^{3+} tags loaded with different metal ions as indicated.

The panels A-C show the data obtained with C2-Ln³⁺ tags at sites A, B, and C, respectively. The spectra were recorded of ca. 150 μM solutions of uniformly ¹⁵N labeled DENpro samples in NMR buffer containing 10% D₂O at 25 °C. Each panel contains three groups of three spectra, where each group shows the result of titration of the tagged protein with increasing amounts of ligand **1** from bottom to top in stoichiometric ratios as indicated. The dashed line identifies the chemical shift of the *tert*-butyl signal of the bound ligand in the diamagnetic samples. This chemical shift is independent of the site of the diamagnetic tag and the same as in wild-type protein. Signals from a non-binding impurity in the ligand stock are labeled with a star. Filled rhombuses and triangles mark the chemical shifts of the *tert*-butyl group in samples tagged with C2-Tm³⁺ and C2-Tb³⁺, respectively. Note the increase of the *tert*-butyl resonance of bound ligand **1** with increasing ligand concentrations, but also that the *tert*-butyl resonance is difficult to assign in panels A and B due to spectral changes induced in the protein NMR spectrum upon ligand binding as well as PREs associated with paramagnetic metal ions.

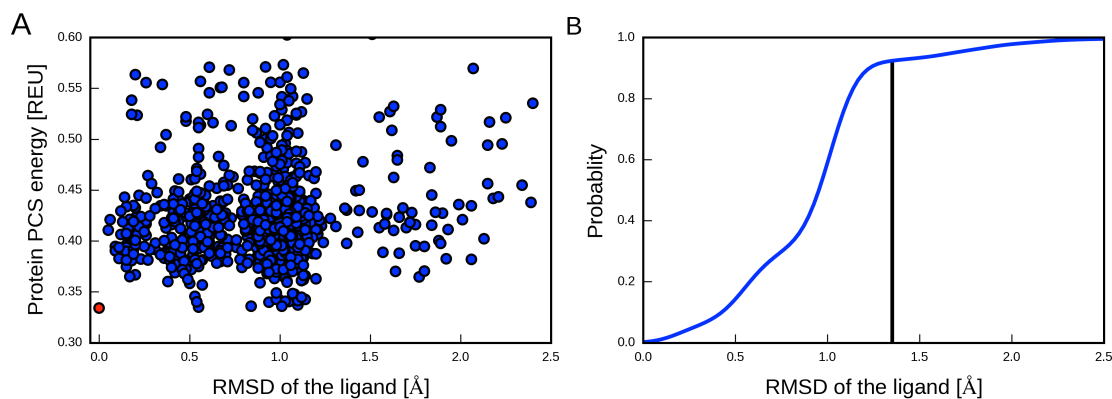


Figure S6. PCS energies and RMSDs of the ligand poses after all-atom Rosetta refinement. (A) PCS energy of the protein (in Rosetta energy units) vs RMSD of the ligand to the final pose (highlighted in red). 1000 structures were produced by the Rosetta refinement protocol, which were all very similar and showed very similar PCS energies. The final ligand pose and protein structure was chosen as the protein-ligand complex with the lowest PCS energy of the protein. The RMSD was calculated for heavy atoms of the ligand only. All ligand poses were within 2.5 Å from the best pose. (B) Probability density plot of the ligand RMSDs with respect to the final docked pose of the ligand. The vertical bar shows that about 92% of the ligand poses are within 1.3 Å from the best pose.

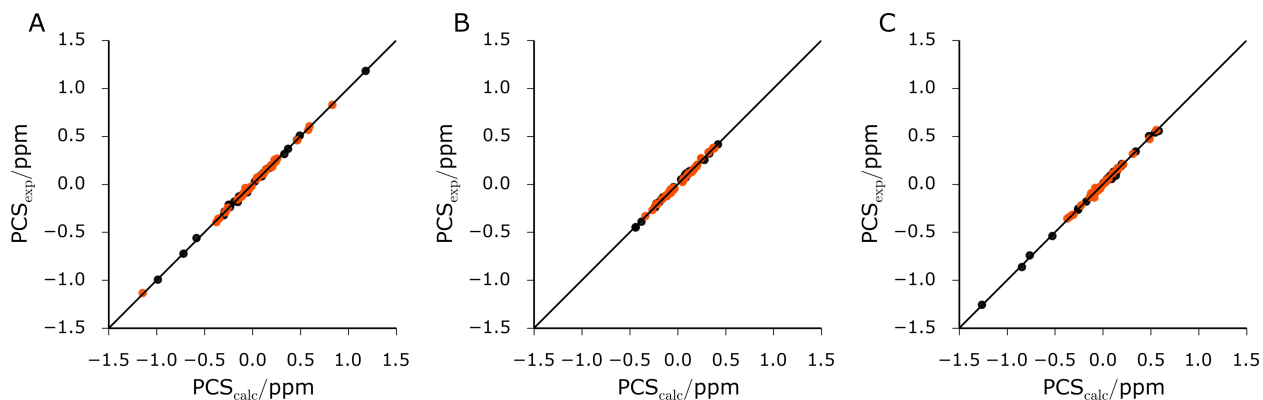


Figure S7. Correlation between experimental and back-calculated PCSs fitted on the model structure. The data from C2-Tm³⁺ and C2-Tb³⁺ tags are shown as red and black points, respectively. (A)-(C) are the correlation plots drawn for the three different mutants A, B, and C, respectively. The $\Delta\chi$ tensor parameters are reported in Table S3.

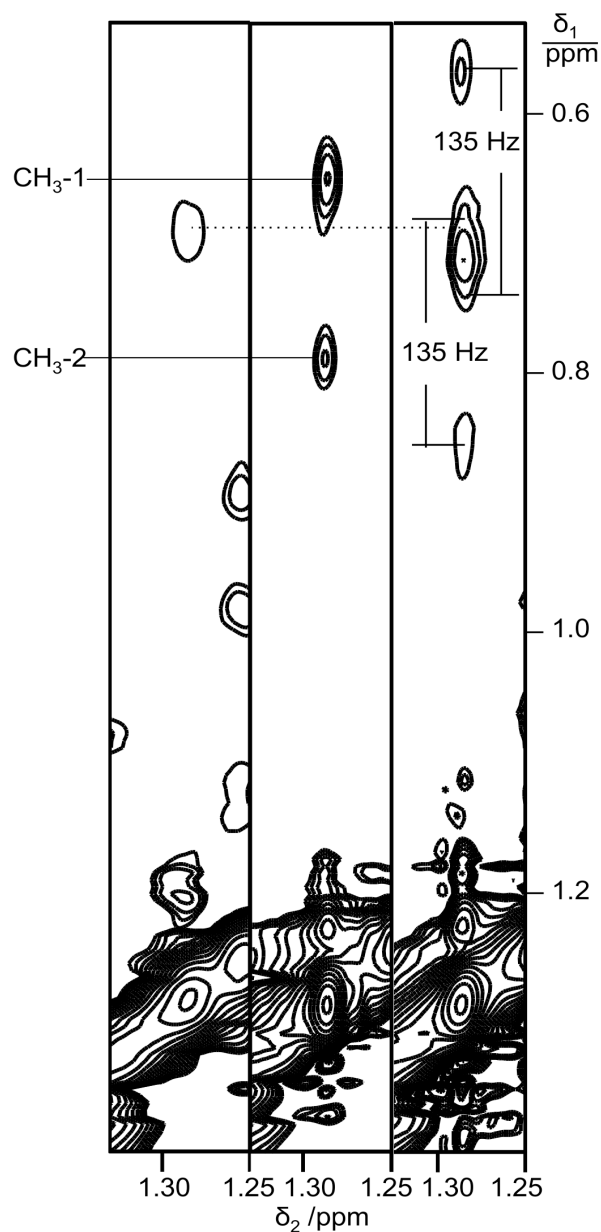


Figure S8. Selected spectral region of NOESY spectra of DENpro in complex with ligand **1**, showing cross-peaks between the methyl groups of Val and the *tert*-butyl resonance of the ligand. The left-most panel shows the spectrum recorded with ligand **2**, which is devoid of a *tert*-butyl group. The center and right panels show the spectra of complexes of ligand **1** with unlabeled DENpro and DENpro prepared with $^{13}\text{C}/^{15}\text{N}$ -labeled valine, respectively. The cross-peaks are clearly split by $^1J_{\text{CH}}$ couplings in the spectrum with isotope-labeled valine. The chemical shifts of the cross-peaks in the indirect dimensions identify the cross-peaks as NOEs with methyl groups of valine.

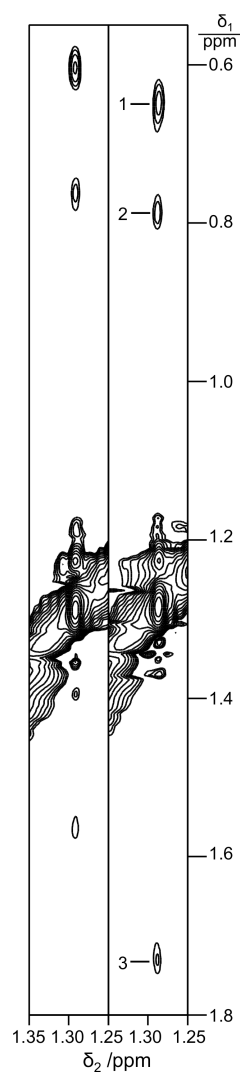


Figure S9. Assignment of NOEs between methyl groups of protein side chains and the *tert*-butyl group of ligand **1**. Right panel: zoom into the spectral region from the NOESY spectrum shown in Figure 2B of the main text. Cross-peaks with the *tert*-butyl resonance of ligand **1** are numbered as in Figure 2B. Left panel: same as the right panel, except for the complex of ligand **1** with the mutant Val155Ile of DENpro rather than wild-type DENpro. Note that the cross-peaks of the Val155Ile mutant display no splitting by $^1J_{\text{HC}}$ couplings, although the protein had been prepared with ^{13}C -labeled valine and the spectrum was recorded without ^{13}C -decoupling. This result indicates that the cross-peaks 1–3 in wild-type DENpro are with Val155 rather than Val154, and that the corresponding cross-peaks observed in the Val155Ile mutant are with isoleucine. The localization space of the *tert*-butyl group shown in Figure 4 of the main text is not near any other methyl group of DENpro. Also note that all NOESY cross-peaks with the *tert*-butyl group are slightly shifted because of a small change in its chemical shift, providing an independent means of identification beyond their narrow line width in the detection dimension.

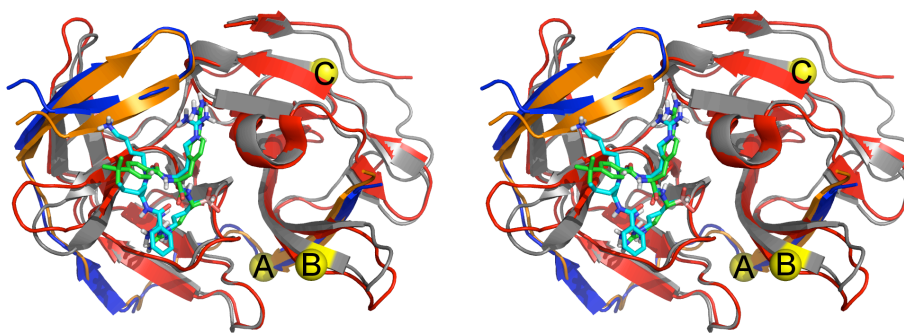


Figure S10. Stereo view comparing the crystal structure of serotype 3 with peptide inhibitor (PDB code 3U1I),³ and the Rosetta-refined model structure of DENpro in complex with ligand **1** determined in the present work. The Rosetta all-atom refinement adjusted the conformation of the backbone atoms around the ligand binding site both for NS2B and NS3pro. NS2B and NS3pro of the crystal structure are shown in blue and red, respectively, with the peptide ligand shown in a stick representation with a cyan backbone. NS2B and NS3pro of the model are shown in orange and grey, with ligand **1** in a stick representation with green backbone atoms. Nitrogen and oxygen atoms are shown in dark blue and red, respectively. Yellow balls mark the sites A-C mutated to cysteine for attachment of C2-Ln³⁺ tags. The backbone of ligand **1** closely aligns with the backbone of the peptide ligand in the crystal structure. The Rosetta all-atom refinement resulted in a small shift of the C-terminal two-stranded β -sheet of NS3pro (residues 154-164) and of the C-terminal β -strand of NS2B (residues 73*-83*) towards the ligand.

References

- (1) Schmitz, C.; Stanton-Cook, M. J.; Su, X.-C.; Otting, G.; Huber, T. *J. Biomol. NMR* **2008**, *41*, 179–189.
- (2) Graham, B.; Loh, C. T.; Swarbrick, J. D.; Ung, P.; Shin, J.; Yagi, H.; Jia, X.; Chhabra, S.; Barlow, N.; Pintacuda, G.; Huber, T.; Otting, G. *Bioconjugate Chem.* **2011**, *22*, 2118–2125.
- (3) Noble, C. G.; Seh, C. C.; Chao, A. T.; Shi, P. Y. *J. Virol.* **2012**, *86*, 438–446.